Additive Manufacturing of Interdigital Filters with Arbitrary Line Cross-Section

Johannes J.P. Venter, *Student Member, IEEE,* Riddhi Maharaj, and Tinus Stander, *Senior Member, IEEE*

***Abstract*— This work investigates the novel use of additive manufacturing in the production of interdigital cavity filters. It is found that AM enables the production of interdigitated pins of complex cross-sectional geometry, leading to the development of a suitable synthesis method using a commonly available 2D Eigenmode port impedance solver. The method is validated by manufacturing an L-band interdigital filter of 70 % fractional bandwidth with triangular bars though selective laser melting, as well as a classical design using rectangular bars. It is found that triangular bars obtain similar coupling to rectangular bars over an average of 35 % wider spacing gaps, reducing its sensitivity to manufacturing error. In addition, neither filter requires post-production tuning, although the bars do warp slightly during printing. These results illustrate the advantages of using additive manufacturing for the synthesis of wideband interdigital filters.**

***Index Terms*— Additive manufacturing, band-pass filters, interdigital filters, microwave filters, selective laser melting, TEM-line filters, wideband filters.**

I. Introduction

Additive manufacturing (AM) has become a popular manufacturing option for microwave devices due to the increased flexibility in realizable geometries compared to conventional subtractive methods [1]. AM processes also have lower lead times and costs [2], [3]. Microwave components may either be printed using a polymer and then metal-plated as a post-production step, such as in stereolithography (SLA) or printed directly in metals, as is the case with selective laser melting (SLM) [1]. SLM is a powder bed fusion process that can produce parts in aluminium or titanium without the need to utilize machining tools [2]. A drawback of this process is that the quality of the surface roughness is low in comparison with machined parts, typically requiring post-process plating of silver for applications at high frequencies [1].

Until now, the main focus in published literature in this area has been on the reduction of size and cost of waveguide components [1], [2]. With the extended capabilities of SLM, it is possible to combine multiple components into one part [3] or to implement parts using novel geometries [1], [2]. What has not yet been investigated, however, is the use of AM in the realisation of novel cavity stripline structures; in particular, interdigital TEM-line filters. These filters can realize low loss and large fractional bandwidths exceeding an octave, making this topology ideal for wideband systems.

Traditionally, interdigital structures have been implemented using either rectangular [4] or circular [5] bars, as standard design tables are only available for those two shapes. More recent synthesis methods do allow for arbitrarily shaped bars, but require either full-wave EM simulations or static field solvers to determine the required line spacings [6], [7].

This work investigates, for the first time, the production of interdigital filters of complex cross-sectional geometry through AM. It further outlines a method whereby the static capacitance and line impedances are calculated using a common 2D Eigenmode port solver, to aid in the synthesis of coupled lines of arbitrary cross-section. The combination of synthesis and manufacturing method leads to an interdigital filter using triangular bars for the first time, which is shown to be less sensitive to process variation than rectangular bars.

The outline for this paper is as follows:
Firstly, a brief discussion is provided of the selected SLM manufacturing process. Secondly, a brief theoretical framework for the synthesis of interdigital filters is presented, including the key theoretical equivalence of coupled line port impedance to static capacitance of lines with equal self-capacitance. Next, the synthesis procedure applied to the prototype devices is outlined, and finally, two prototypes are presented: a classical example from literature [8] using rectangular coupled bars, and a novel geometry using triangular bars. In all cases, CST Microwave Studio 2018 is used for simulation.

II. Manufacturing and Assembly

A. SLM Manufacturing Process

The SLM process is a well-known, well-documented additive manufacturing process [9], [10], that is gaining popularity for the manufacture of RF components [11].

The printer properties of the printer used in this project are defined in Table I. The critical process parameters are the laser power, laser scan speed, laser scan pattern, particle size and packing density as well as layer uniformity and thickness [12]. These parameters are all pre-set by the SLM Solutions software, based on the material in use, layer thickness, and laser power

Manuscript received August 28, 2019; revised 23 October 2019. The authors wish to thank CST AG for the use of CST Microwave Studio under the academic license agreement. This work was supported by the Eskom Tertiary Education Support Programme (TESP) and the National Research Foundation of South Africa (NRF) under grants 92526 and 93921.
Digital Object Identifier: 10.1109/TCPMT.2020.2967807

J.J.P. Venter and T. Stander are with the Carl and Emily Fuchs Institute for Microelectronics (CEFIM) in the Department for Electrical, Electronic, and Computer Engineering at the University of Pretoria, Pretoria, South Africa (email: venter.jjp@tuks.co.za; tinus.stander@up.ac.za).
R. Maharaj is with NewSpace Systems, Cape Town, South Africa (email: rm@newspacesystems.com).

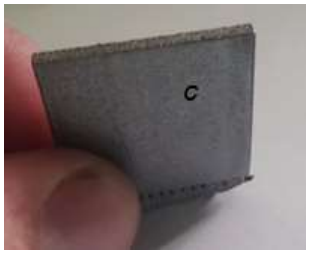

(a) Vertically oriented geometry.

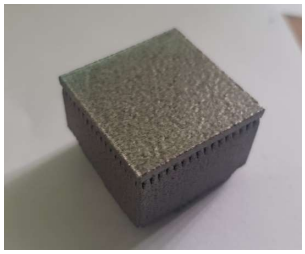

(b) Horizontally oriented geometry.

Fig. 1. Illustration of printed geometries for determination of surface roughness.

available. These are automatically set to achieve a single melt vector that can fuse completely with the neighbouring melt vectors and the preceding layer [9], resulting in maximum density that ultimately determines the quality of the part.

Energy density is directly related to the melt density. The density is, therefore, analysed after sampling various parameters (using the SLM Solutions software) by varying the energy density of the parameters, and final build parameters are selected for which energy density yields the best material density. It takes into consideration the spot size (mm), the laser speed (mm/s), and the layer thickness (mm). For this build, the layer thickness is constant (30 µm) and the spot was pre-set from build parameters, leaving laser power and scan speed as optimized parameters to achieve optimal density. The deposition or build rate is determined by using the energy density parameter.

The metal alloy used was SLM Solutions $AlSi_{10}Mg$, which is a common casting alloy. $AlSi_{10}Mg$ features high corrosion resistance, low density, good weldability, good castability, and high thermal and electrical conductivity [2], [13]. In a process optimization study [14], it was found that the quality of SLM components also dependent on powder morphology and content, and not just the processing parameters. Small and spherical powders with higher silicon content gave a higher relative density in the SLM components than larger irregular shaped powders [9]. The metal powder properties for the powder used here are specified in Table II.

To obtain accurate surface roughness measurements, flat sheets were printed in the build orientation of the filters (Fig. 1) and measured using a surface roughness profilometer. Table III summarizes the surface roughness measured.

TABLE I
PRINTER PROPERTIES

Printer type	SLM280 2.0; 400 W Single Laser
Melt density	99.97 % (According to SLM Parameters)
Powders used	$AlSi_{10}Mg$
Build vat shape	Square
Build volume	280 x 280 x 320 (mm) (L x W x H)
Laser power	SLM Pre-set (from parameter files)
Spot beam	Specified at 70 µm
Layer thickness	30 µm
Processing atmosphere	Max 2% O_2, Full argon environment
Minimum printable hole size / wall thickness	Estimated at 0.35 mm for $AlSi_{10}Mg$.

TABLE II
$ALSI_{10}MG$ METAL POWDER PROPERTIES (SLM SOLUTIONS MATERIAL DATASHEET)

Particle size distribution	20 – 60 µm
Grain shape	Spherical
Density	2.68 g/cm^3
Bulk thermal conductivity at 20 °C	130 – 150 W/mK
Bulk electrical resistivity*	16000000 S/m

* Value obtained from [15].

TABLE III
SURFACE ROUGHNESS DETERMINATION

	Vertical (90 degrees)	Horizontal (180 Degree)
Picture	Fig. 1(a)	Fig. 1(b)
Surface roughness	2.7 µm	1.2 µm
Interdigital filter reference	Orientation of the internal wall surfaces of the filter cavity and the filter bars.	Orientation of the filter cavity floor and lid.

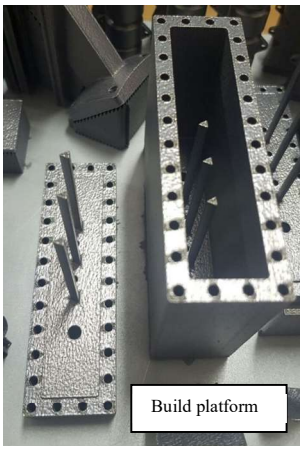

Fig. 2. Interdigital filter, using triangular bars, placement on build platform.

For the 3D printing of the interdigital filters, each component was split into four parts, a top part (cover) and a bottom part (cavity), as well as two individual filter bars which were attached to the two filter connectors. Fig. 2 shows the orientation of the components on the build platform, with the cover placed on the left and the cavity on the right. The parts were orientated perpendicular to the build platform, such that

the cavity could be printed without internal supports, and the cover was orientated such that the filter bars were built in the vertical direction, again to avoid any overhanging areas. It is important to note that no post-processing (plating) was done to improve the surface roughness.

B. Assembly

Once the individual parts have been produced, the printed mounting holes for the connector flanges were tapped with M2.5 thread, as well as the M3 holes for the cavity assembly screws. At the top of each of the two external coupling bars, a blind hole with a diameter of 1.3 mm was drilled for the SMA panel jack receptacle's centre conductor, as shown in Fig. 3. The connectors' extended Teflon probes were cut to length (with the dielectric trimmed flush with the internal cavity), the coupling bars press-fitted to the connectors, and the assembly then fitted through the printed connector holes in the lid and cavity parts. The two parts were then assembled with 28 M3 screws of 4.7 mm pitch along the cavity periphery.

The air gaps introduced along the assembly seam (due to surface roughness on both the lid and cavity parts) was considered negligible at the frequency range of interest.

III. Filter Synthesis

A. Capacitance Matrix Synthesis

The method used to synthesise the interdigital filters in this work (Fig. 4) is based on the method developed by Matthaei [8], though the exact method of Wenzel [16] could be applied. Application of this method for a given filter order, Chebyshev prototype function [6] pass band ripple, centre frequency and fractional bandwidth, will produce a series of normalized self-capacitance $C_{k/\varepsilon}$ and mutual-capacitance $C_{k,k+1/\varepsilon}$ values. This method is iterated until a total capacitance value (C_{total}) of approximately 5.4 is reached, to yield optimum resonator Q-factor. We further apply the capacitance matrix assembly and equalization detailed in [17] to achieve uniform self-capacitance (and, subsequently, uniform bar dimensions) throughout the filter.

B. Determination of Geometry

With the capacitance values (with optimal line Q-factors) determined, the physical implementation can follow. For the rectangular bar prototype [8], the synthesis procedure in [4] may be followed to find initial dimensions for t, W, G_{ij} and W_s (Fig. 4(b)), while similar methods exist for round bars [5]. However, as additive manufacturing allows for the creation of bars of arbitrary cross-sectional dimension, a method that does not rely on analytical solutions or design graphs is applied.

In this work, the static capacitance values C_k and $C_{k,k+1}$ obtained previously are transformed to even- and odd-mode static capacitances C_{0e} and C_{0o} [15], which are then related to even- and odd-mode impedances Z_{0e} and Z_{0o} [15,16].

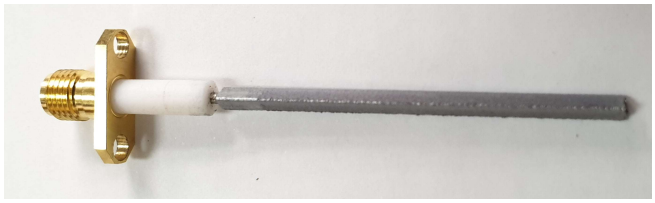

Fig. 3. Close-up of connector and outer resonator assembly, after press fitting.

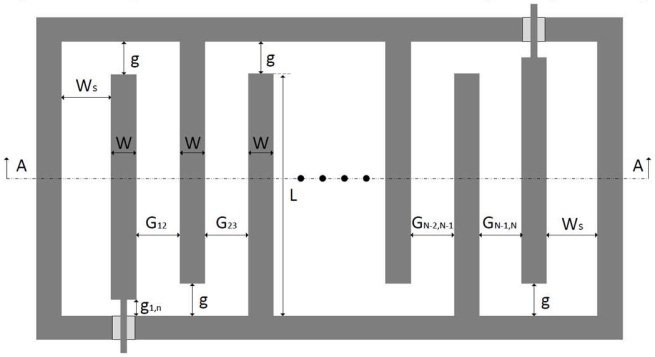

(a) Cross-sectional top view of interdigital filter layout.

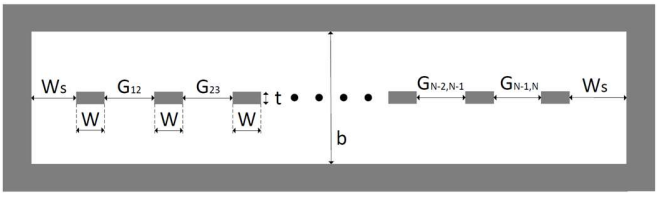

(b) Cross-sectional side view of interdigital filter, rectangular bars, layout.

Fig. 4. Cross-sectional views of interdigital filter layout.

Next, the cross-sectional geometry of a single line is drawn in a 2D Eigenmode port solver (Fig. 5) deriving the self-capacitance C_{0e} from the simulated TEM port impedance Z_0. If lines have dissimilar self-capacitance from the synthesis method, these need to be equalised beforehand using the method in [17].

With the line and ground spacing dimensions now fixed, a second identical line is introduced to the port. The lines are excited the common and differential modes (as shown in Fig. 6) to calculate Z_{0e} and Z_{0o}. The distance between the lines are tuned until the required even- and odd-mode impedances are obtained, and the procedure repeated for each coupled line pair. The left- and right-hand side ground planes far enough ($\approx 3b$) away from the coupled line structure to allow for minimal coupling of the electric field to these planes. This is done to ensure accurate calculation of Z_{0e} and Z_{0o}.

Once the cross-sectional geometries have been established, the initial line length L (Fig. 4(a)) is selected as $\lambda_g/4$, where the propagation constant extracted from the prior 2D Eigenmode port solver is used to determine λ_g.

The resulting filters were then 3D simulated using the frequency domain solver in CST Microwave Studio, and the geometry fine-tuned.

IV. Comparison of Approaches

To illustrate the advantages that AM (and the applied synthesis method) hold in the design of interdigital filters, a comparative analysis of coupling between conventional rectangular bars [4], and a novel triangular bar geometry, is conducted, For the purposes of this analysis the self- and mutual-capacitances were chosen to be $C_{11} = C_{22} = 1.698$ and $C_{12} = 1.500$. The impedance of the coupled lines, and the spacing between the lines, were determined using the method described in Section III.B. The nominal line spacing for the rectangular and triangular lines are 2.38 mm and 3.32 mm, respectively, with other dimensions as presented in Section V.

The results of this analysis (Fig. 7) indicate that the coupled triangular bars have less 11.36% less variation in C_{12} compared to the rectangular bars for the same ±0.5 mm variation in coupled line spacing (ΔG_{12}). This is due to the same mutual capacitance being achieved over a longer coupling distance. This increase in line spacing can be leveraged to ease the required manufacturing tolerances or enable the realisation of filters with wider bandwidths. The geometry that enables this improvement is, in turn, the result of the unique manufactured geometries possible with AM, with a suitable synthesis method. In this case, triangular bars would be impractical to machine horizontally without a course staircase approximation (Fig 8(a)) and impossible to machine vertically due to the required machining depth (Fig. 8(b)).

V. Measurement Results

A. Rectangular Bar Filter

To validate the proposed method, the coupled rectangular bar filter in [8] is first replicated. The filter is of order $N = 8$, has a 70% fractional bandwidth centred at $f_0 = 1.5$ GHz and 0.1 dB passband ripple. Given these requirements, the normalized self- and mutual capacitance values are calculated as shown in Table IV.

Using the method described in Section III, the rectangular bar dimensions for the replicated filter are set to $t = 1.6$ mm, $W = 3.19$ mm, and $L = 46.18$ mm (referring to Fig. 4). The enclosure spacings of the design in [8] were used, resulting in $b = 15.875$ mm, $g = 3.810$ mm, $g_{1,n} = 1.905$ mm, and $W_s = 19$ mm. Finally, 50 Ω coaxial connections to the exterior bars are added to excite the filter.

Table V presents the results obtained for the line spacings using the applied method, and those using the method in [8]. Full-wave simulation results are obtained using CST Microwave Studio's frequency domain solver, with lossy materials and the surface roughness specified in Table III. The close correspondence between the initial and tuned simulation dimensions validates the use of the simplified method in [8] , as opposed to the exact synthesis method in [16].

All measurements were carried out on an Anritsu ME4647A VNA, with the measurement setup shown in Fig. 9. The calibration plane was placed at the SMA connector face, with the Anritsu 36585 series AutoCal unit used for calibration.

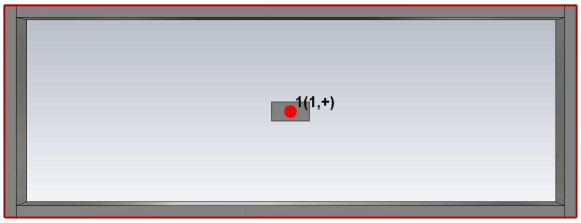

Fig. 5. CST port setup for determination of single line impedance (step 1).

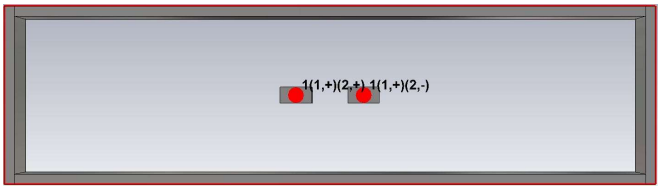

Fig. 6. CST Port setup for determination of common and differential mode impedances (step 2).

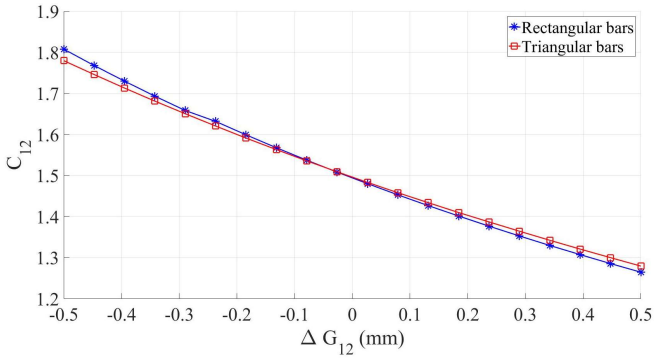

Fig. 7. Comparison of C_{12} variation between rectangular and triangular bars for a variation in bar spacing ranging of -0.5mm to 0.5mm from the nominal value.

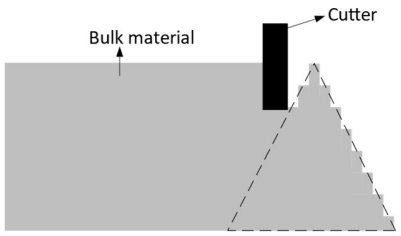

(a). Staircase approximation needed for traditional machining of triangular bar geometry.

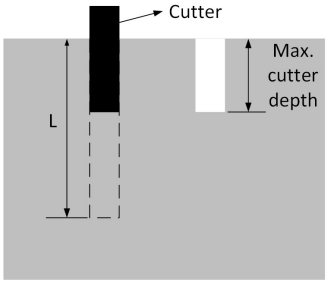

(b). Illustration of limited machining depth of traditional machining methods.

Fig. 8. Limitations of traditional machining methods when manufacturing triangular bars.

TABLE IV
SELF- AND MUTUAL-CAPACITANCE VALUES FOR FILTER DESIGNS

Parameter	Value
C_1 & C_8	1.698
C_2 & C_7	1.709
C_3 & C_6	1.707
C_4 & C_5	1.707
C_{12} & C_{78}	1.400
C_{23} & C_{67}	1.052
C_{34} & C_{56}	1.046
C_{45}	1.036

TABLE V
INTER-COUPLED LINES SPACING FOR REPLICA DESIGN

	[8] (mm)	2D initial (mm)	3D tuned (mm)	Δ (%)
G_{12} & G_{78}	2.337	2.400	2.380	-0.837
G_{23} & G_{67}	3.493	3.550	3.520	-0.847
G_{34} & G_{56}	3.651	3.550	3.692	3.922
G_{45}	3.733	3.550	3.692	3.922

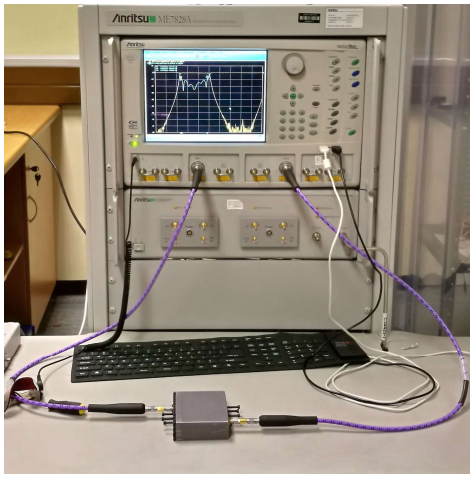

Fig. 9. Coaxial measurement setup.

There is good agreement in filter bandwidth and passband return loss between the simulated responses of the reference filter and the filter synthesized using the applied method (Fig. 10). The proposed method yields accurate initial starting conditions, which require minimal (maximum of 4%) tuning to yield a satisfactory design. The measurement results of the prototype filter are also shown in Fig. 10, indicating good agreement between simulation and measurement in terms of bandwidth, but increased port reflection and passband ripple. These discrepancies are due to process variations, as the filter was not tuned post-production. The stopband response of the prototype, both in simulation and measurement, closely tracks the response of the reference filter.

B. Triangular Bar Filter

To illustrate the flexibility of AM in bar shape construction, as well as the applied synthesis method, an interdigital filter using triangular bars (Fig. 11) as coupled lines was synthesized to the same specifications as the previous example. To realize the required line impedance specified, the line dimensions are set to H = 3.1 mm, W = 3 mm, and L = 46.18 mm. The enclosure spacings (b, g, $g_{1,n}$ and W_s) are kept the same as in the previous design.

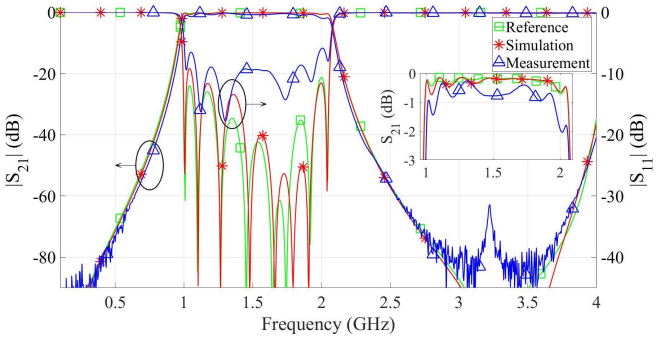

Fig. 10. S-parameter measurement results of replica filter, using square coupled lines, compared with simulation and reference (from [8]) response.

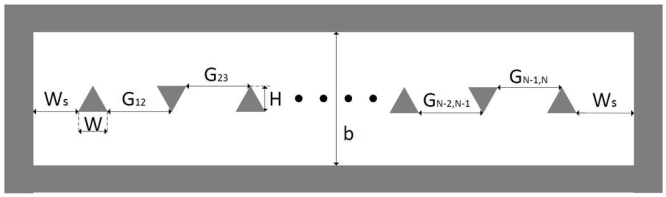

Fig. 11. Cross-sectional side view of interdigital filter, with triangular bars, layout.

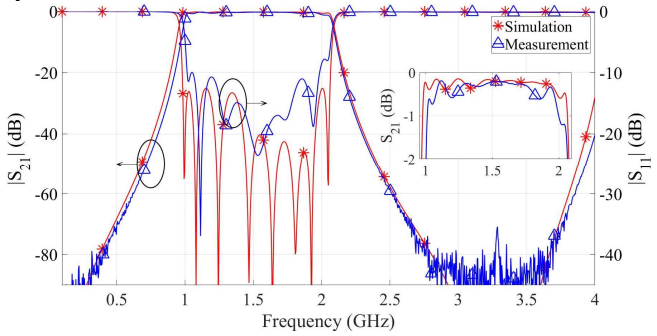

Fig. 12. S-parameter measurement results of triangular coupled line filter compared with simulated response.

TABLE VI
INTER-COUPLED LINES SPACING FOR TRIANGULAR BAR DESIGN

	2D FEM initial (mm)	Final filter tuned (mm)	Δ (%)
G_{12} & G_{78}	3.450	3.322	-3.781
G_{23} & G_{67}	4.650	4.670	0.429
G_{34} & G_{56}	4.650	4.910	5.439
G_{45}	4.650	4.910	5.439

Table VI presents the initial line spacings compared with the final tuned spacings. The results indicate that the proposed method yields good initial starting conditions with a maximum of 5.44 % change required in reaching the final dimensions.

The S-parameter results of the triangular bar filter are shown in Fig. 12. Minor bandwidth reduction (from 76.1 % to 72.6 %) can be observed at the low frequency cut-off. Less than -10 dB return loss is achieved across most of the prescribed bandwidth, with some degradation near the upper cut-off. The insertion loss of the prototype closely tracks that of the simulation results, with some increase in insertion loss at the band edges. The stopband response of the prototype corresponds well to the simulated response.

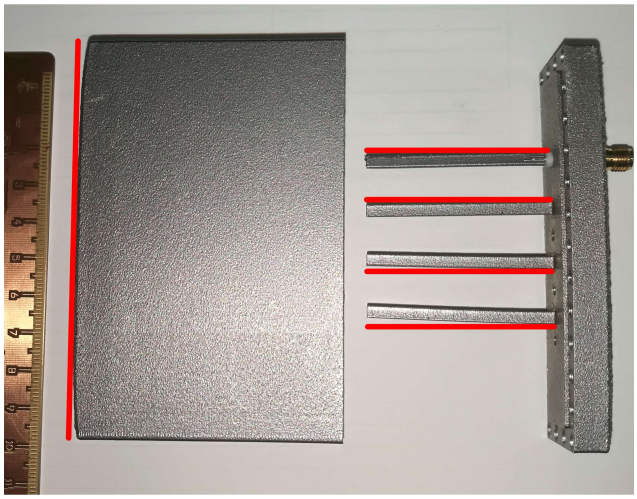

Fig. 13. Top-view of rectangular bar filter prototype, illustrating deformation of cavity and internal filter fingers.

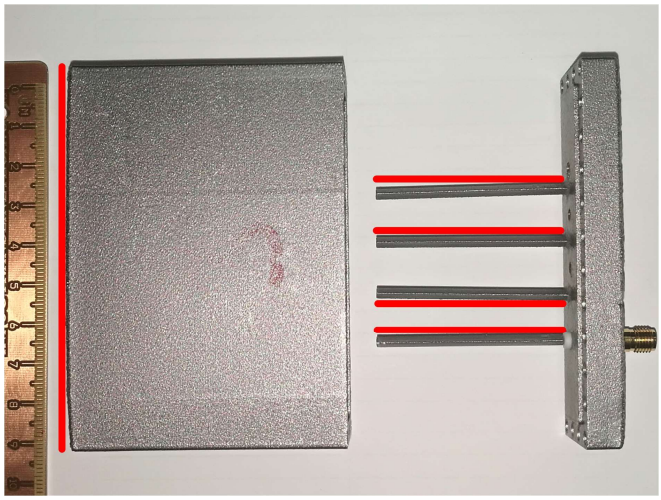

Fig. 14. Top-view of triangular bar filter prototype, illustrating deformation of cavity and internal fingers.

C. *Comparison Between Manufactured Prototypes*

From the measured results of the two prototypes, it is evident that the triangular bar filter better approximates the simulated response. Although both filters suffer from slight de-tuning, the impact is less severe in the triangular bar filter prototype. This is due to the triangular line geometry, which requires gap widths that are, on average, 34.56 % wider compared to that of the rectangular bar filter. This reduced sensitivity to manufacturing tolerance demonstrates one possible advantage of designing interdigital filters with arbitrarily shaped coupled lines, as is possible with AM and a suitable synthesis method.

There is also a 7.34 % reduction in overall width for the triangular bar filter (89.42 mm) compared to the width of the rectangular bar filter (96.5 mm). Although a reduction in size was not the primary objective of this design, it illustrates that by changing the geometry of the coupled lines, a reduction in overall filter size can be achieved.

Some deformation due to the AM process is evident in Figs. 13 and 14. Vernier measurements of the deformation indicated that the maximum amount of error between adjacent bars on the same ground plane was equal to 0.98 mm (for the lower two bars of the rectangular bar filter in Fig. 13). Post-analysis of the deformation was performed in simulation using a 125 sample Monte Carlo run, with a maximum displacement ranging from -0.5 mm to 0.5 mm at the bar tips, assuming no error in positioning of the base of the bar. These results, shown in Figs. 15 and 16, indicate that the measured results fall within the expected performance bounds, considering typical manufacturing tolerance for the process. It is found that manufacturing tolerance introduces worst-case variation in in-band insertion loss of 2.1 dB for the rectangular bar filter and 1.7 dB for the triangular bar filter, with minimum return loss (across the band) variation of 3.73 dB and 4.19 dB for the two filters, respectively . The 60 MHz bandwidth reduction is, however, not accounted for. The discrepancy between simulation and measurement observed in Figs. 10 and 12 can, therefore, be attributed primarily to standard process tolerances and bar deformation.

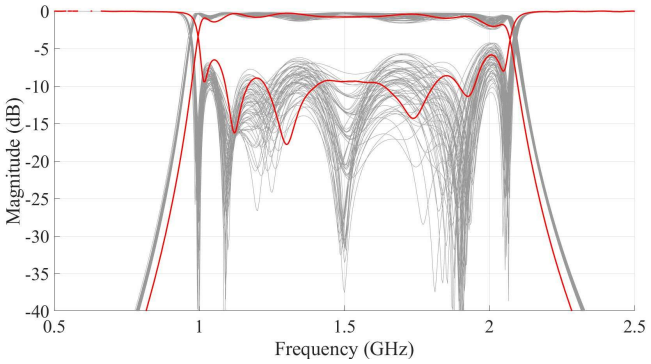

Fig. 15. S-parameter results for rectangular bar filter, as well as Monte Carlo analysis responses, considering only deformation on coupled lines.

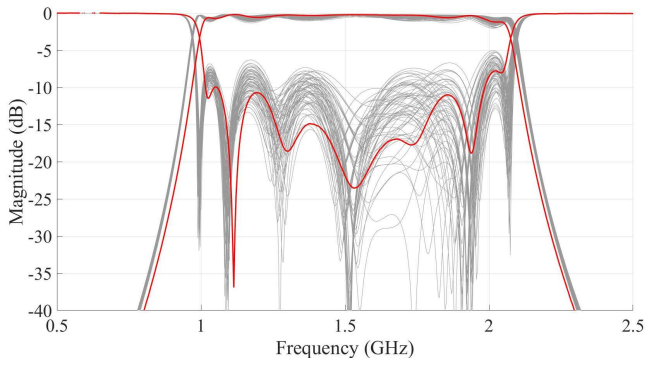

Fig. 16. S-parameter results for triangular bar filter, as well as Monte Carlo analysis responses, considering only deformation on coupled lines.

VI. Conclusion

In this paper, it is shown that SLM is a viable process for manufacturing wideband interdigital filters with arbitrary bar geometries, which is not possible with conventional subtractive machining methods. To facilitate development of such wideband interdigital filters with arbitrary bar geometries, a simple synthesis procedure is presented based on readily available 2D Eigenmode port solvers. This method results in

good first-iteration dimensions for bar spacing with minimal full-wave tuning needed to reach a satisfactory design. The approach is shown to achieve similar results, compared to conventional methods, with conventional rectangular bar geometry, and is also shown effective in synthesising filters with arbitrary cross-sectional line geometries. It is also shown that using bars with arbitrary geometries may reduce the filter's size and susceptibility to process variations. This is illustrated with improved first-iteration performance of the triangular bar filter over a rectangular bar filter.

The deformation of the filters in Figs. 13 and 14 are of some concern, especially as a statistically significant number of sample prototypes could not be produced to verify repeatability of the error. This will be further investigated in future work. Further future work will investigate the suitability of other processes, such as metal-plated SLA-printed parts [19] or Binder Jetting [20], in realizing interdigital cavity filters. Different polishing and plating options [21] could also then be investigated. Finally, as it is widely known that loss due to surface roughness increases with frequency [22], it is proposed that a mm-wave prototype is produced in future work, to investigate the geometry and process's relative performance *vis-à-vis* waveguide filters in similar processes and frequency ranges.

ACKNOWLEDGMENT

The authors wish to thank Prof. P. W. van der Walt for his valuable contributions in the preparation of this manuscript, and NewSpace Systems for sponsoring the manufacturing of the prototypes.

REFERENCES

[1] P. A. Booth and E. V. Lluch, "Realising Advanced Waveguide Bandpass Filters using Additive Manufacturing," *IET Microw. Antennas Propag.,* vol. 11, no. 14, pp. 1943-1948, 2017.

[2] O. A. Peverini, M. Lumia, F. Calignano, G. Addamo, M. Lorusso, E. P. Ambrosio, D. Manfredi and G. Virone, "Selective Laser Melting Manufacturing of Microwave Waveguide Devices," *Proceedings of the IEEE,* vol. 105, no. 4, pp. 620-631, 2017.

[3] O. A. Peverini, M. Lumia, G. Addamo, F. Paonessa, G. Virone, R. Tascone, F. Calignano and D. Manfredi, "Integration of an H-Plane Bend, a Twist, and a Filter in Ku/K-Band Through Additive Manufacturing," *IEEE Trans. Microw. Theory Tech.,* In Press.

[4] W. J. Getsinger, "Coupled Rectangular Bars Between Parallel Plates," *IRE Trans. Microw. Theory Tech.,* vol. 10, no. 1, pp. 65-72, 1962.

[5] E. G. Cristal, "Coupled Circular Cylindrical Rods Between Parallel Ground Planes," *IEEE Trans. Microw. Theory Tech.,* vol. 12, no. 7, pp. 428-439, 1964.

[6] J. S. Hong and M. J. Lancaster, Microstrip Filters for RF/Microwave Applications, New York: John Wiley and Sons, 2001.

[7] W. P. du Plessis, "Interdigital Filter Design," *Microw. Opt. Technol. Lett.,* vol. 51, no. 10, pp. 2269-2272, 2009.

[8] G. L. Matthaei, "Interdigital Band-Pass Filters," *IRE Trans. Microw. Theory Tech.,* vol. 10, no. 6, pp. 479-491, 1962.

[9] C. Yap, C. Chua, Z. Dong, Z. Liu, D. Zhang, L. Loh and S. L. Sing, "Review of Selective Laser Melting: Materials and Applications," *Applied Physics Reviews,* vol. 2, no. 4, 2015.

[10] D. Manfredi, F. Calignano, M. Krishnan, R. Canali, E. P. Ambrosio, A. Biamino, D. Ugues, M. Pavese and P. Fino, "Light Metal Application Alloys: Additive Manufacturing of Al Alloys and Aluminium Matrix Composites (AMCs)," Intech, London, 2014.

[11] O. A. Peverini, M. Lumia, F. Calignano, G. Addamo, M. Lorusso, E. P. Ambrosio, D. Manfredi and G. Virone, "Selective Laser Melting Manufacturing of Microwave Waveguide Devices," *Proceedings of the IEEE,* vol. 105, no. 4, pp. 620-631, 2017.

[12] J. Hart, "Additive Manufacturing (Lecture Slides: MIT)," SlideShare, 21 Nov. 2016. [Online]. Available: https://www.slideshare.net/AJohnHart/additive-manufacturing-2008x-lecture-slides. [Accessed 1 May 2018].

[13] "Additive Manufacturing: A Guide to Metals Used in Additive Manufacturing," GE Additives, 2018. [Online]. Available: https://www.ge.com/additive/additive-manufacturing/information/metal-additive-manufacturing-materials. [Accessed 1 May 2018].

[14] K. Kempen, L. Thijs, E. Yasa, M. Badrossamay, W. Verheecke and J. Kruth, "Process Optimisation and Microstructural Analysis for Selective Laser Melting of AlSi10Mg," in *Solid Freeform Fabrication Symposium*, Austin, TX, USA, 2011.

[15] J. Lorente, M. Mendoza, A. Petersson, L. Pambaguian, A. Melcon and C. Ernst, "Single Part Microwave Filters Made From Selective Laser Melting," in *Proc. 39th European Microwave Conf.*, Rome, Italy, 2009.

[16] R. J. Wenzel, "Exact Theory of Interdigital Band-Pass Filters and Related Coupled Band-Pass Structures," *IEEE Trans. Microw. Theory Tech.,* vol. 13, no. 5, pp. 559-575, 1965.

[17] R. J. Wenzel, "Theoretical and Practical Applications of Capacitance Matrix Transformations to TEM Network Design," *IEEE Trans. Microw. Theory Tech.,* vol. 14, no. 12, pp. 635-647, 1966.

[18] W. J. D. Steenaart, "The Synthesis of Coupled Transmission Line All-Pass Networks in Cascades of 1 to n," *IEEE Trans. Microw. Theory Tech.,* vol. 11, no. 1, pp. 23-29, 1963.

[19] M. D'Auria, W. J. Otter, J. Hazell, B. T. W. Gillatt, C. Long-Collins, N. M. Ridler and S. Lucyszyn, "3-D Printer Metal-Pipe Rectangular Waveguides," *IEEE Trans. Compon. Packag. Manuf. Technol.,* vol. 5, no. 9, pp. 1339-1349, 2015.

[20] E. A. Rojas-Nastrucci, J. T. Nussbaum, N. B. Crane and T. M. Weller, "Ka-Band Characterization of Binder Jetting for 3-D Printing of Metallic Rectangular Waveguide Circuits and Antennas," *IEEE Trans. Microw. Theory Tech.,* vol. 65, no. 9, pp. 3099-3108, 2017.

[21] S. Maas, Coaxial Resonator Filters, M.S. thesis, Dept. Electrical, Electronic Engineering, University of Stellenbosch, 2011.

[22] G. Gold and K. Helmreich, "A Physical Surface Roughness Model and Its Applications," *IEEE Trans. Microw. Theory Tech.,* vol. 65, no. 10, pp. 3720-3732, 2017.

Johannes J.P. Venter (STM'17) received the B.Eng. degree in Electronic Engineering, and the B.Eng.Hons. degree in Microelectronic Engineering from the University of Pretoria, Pretoria, South Africa, in 2015 and 2016, respectively. He is currently pursuing a PhD degree in Electronic Engineering with the same institution.

His current research interests include millimetre wave phase shifters, oscillation-based testing of phase shifters, dispersive amplitude networks, and slow-wave structures.

Riddhi Maharaj obtained her B.Sc Honours in 2013, her M.Sc in Chemical Engineering in 2015, and is currently pursuing her M.Phil in Space Studies through the University of Cape Town. Her current area of research is focused on the in-situ production of silicon (for photovoltaic production) and oxygen using lunar regolith, for future lunar colonies. Other areas of research include chemical catalysis for bio-based plasticizers, reactor design modelling and metal additive manufacturing. She is also currently working full-time for the advanced manufacturer NewSpace Systems (NSS), where her main responsibility as materials engineer has been leading an R&D project on the additive manufacturing of low-cost, high-frequency RF components. In addition to this, she has also made significant contributions towards the conceptualisation of the NSS component testing laboratory which is set to extend the capabilities of the existing internationally accredited NSS facilities.

Tinus Stander (M'10-SM'13) completed his B.Eng and PhD degrees in Electronic Engineering at the University of Stellenbosch in 2005 and 2009, respectively. From 2010 to 2012 he served as RF and microwave engineer at Denel Dynamics (a division of Denel SOC LTD) before joining the Carl and Emily Fuchs Institute for Microelectronics (Dept. Electrical, Electronic and Computer Engineering) at the University of Pretoria in 2013. He currently serves as principal investigator in microwave and mm-wave microelectronics at the Institute, with personal research interest in the application of distributed passives on-chip and built-in self-testing. He is also registered as Professional Engineer with the Engineering Council of South Africa, and serves as Scientific Advisor to Multifractal Semiconductors (Pty) Ltd.